Mixed layer in a stably stratified fluid

F. Califano, Anne Mangeney

Nonlinear Processes in Geophysics (1994) 1: 199 - 208

Nonlinear Processes in Geophysics

Mixed layer in a stably stratified fluid

F. Califano and A. Mangeney

Observatoire de Paris-Meudon (DESPA), 5 Place Jansen, 92195 Meudon, France

Received 20 June 1994 - Accepted 8 November 1994 - Communicated by A. Provenzale

Abstract. We present a numerical study of the generation and evolution of a mixed layer in a stably stratified layer of Boussinesq fluid. We use an external forcing in the equation of motion to model the experimental situation where the mechanical energy input is due to an oscillating grid.

The results of 2D and 3D numerical simulations indicate that the basic mechanism for the entrainment is the advection of the temperature field. This advection tends to produce horizontally thin regions of small temperature vertical gradients (jets) where the hydrodynamics forces are nearly zero. At the bottom of these structures, the buoyancy brakes the vertical motions. The jets are also characterized by the presence of very short horizontal scales where the thermal diffusion time turns out to be comparable with the dynamics time. As a result, the temperature field is well mixed in a few dynamics times. This process stops when the mechanical energy injected becomes comparable with the energy dissipated by viscosity.

1 Introduction

It is often observed, both in laboratory and geophysical experiments (see for example Turner 1986, Fernando 1991), that when a stably stratified fluid is submitted to some mechanical forcing at the top or bottom boundary, a mixed layer develops in the vicinity of the boundary across which mechanical energy is injected into the fluid. In this layer, the initial stratification of temperature, density, etc., is strongly modified.

It is also observed that the mixed layer is separated from the quiescent region by a thin interface characterized by strong gradients of temperature, density and velocity. Due to the process of entrainment, the interface propagates with a velocity u_e whose ratio to the local "turbulent" velocity u is approximately a constant

$$U = \frac{u_e}{u},$$

which depends on some basic parameters of the system, the Richardson number, Prandtl number, etc (Turner 1973, Thompson & Turner 1975, Linden 1975, Hopfinger & Toly 1975, Fernando & Long 1985).

In order to study this process, the typical laboratory experiment is that of a vertically oscillating horizontal grid inside a tank of stratified fluid (Turner 1968). The vertical penetration of the motions generated by the grid is controlled by a *non classical diffusive process* (Thompson & Turner 1975), and basically there is a *conversion of mechanical energy into potential energy* (Linden 1975). The experiments also show that, in the absence of mean velocity shear, the energy converted into potential energy is proportional to the kinetic energy which is available near the interface, and not to that which is injected by the external forcing. This suggests that to describe correctly the deepening process, one cannot avoid to study in some detail the transfer of mechanical energy from the input region to the vicinity of the interface. This was done in a semi empirical way by Linden (Linden 1975) to reconcile Niiler's classical model (Niiler 1975) with the experimental results. Furthermore, the internal waves generated at the interfacial layer and radiated into the quiescent fluid, may influence the penetration of the mixed layer, as these waves remove free energy which cannot anymore be converted into potential energy.

In order to understand this non-classical diffusive process, a number of models have been proposed, which can be roughly summarized as follows.

In the first type of models, it is assumed that the mixing of the fluid is produced by the recoil of quiescent fluid into the mixed region, recoil produced by the collision of a vertically propagating eddy against the interface (Linden 1973). Then, the balance between the available kinetic energy at the interface and the rate of increase of potential energy, allows to obtain the power

law dependence on the Richardson number R_i of the entrainment velocity, as

$$U \sim R_i^{-3/2},$$

which is observed in the majority of the laboratory experiments.

This "splashing" mechanism has been observed experimentally (Dahm & al. 1989) in the case of small Richardson numbers; at large R_i the eddies tend to flatten near the interface, as if they were colliding with a rigid surface; in this case, it has been recently suggested (Fernando & Long 1985a) that the physical mechanism which produce the mixing of the fluid is interfacial wave breaking.

A second type of models which has been proposed to explain the non-diffusive mixing of stratified fluid, is that of Kelvin-Helmholtz instabilities on small (turbulent) eddies (Mory 1991). In this case, the direct consequence of the growth of the linear instability of the small eddies, is to engulf part of the quiescent fluid and bring it into the well mixed region.

At the moment, none of the existing models discussed above can be considered as satisfactory. For this reason we decide to attack the problem of the generation and evolution of a mixed layer in a stratified fluid from a numerical point of view. In fact, the aim of the paper is to clarify the physics of the process which, in the range of parameters which can be achieved in a numerical simulation, is responsible of the mixing of the fluid.

The paper is organized as follow. In Section 2 we illustrate the dimensionless equations and the mechanical forcing used to simulate the experiments. In Section 3 we present the results of the simulations, which are then discussed in Section 4. Finally, conclusions are presented in Section 5.

2 The equations

Due to the many difficulties which arise for fluid simulations in the case of "strong" perturbations at "high" Reynolds numbers, a number of simplifications in modeling the mixed layer experiment have been introduced in the numerical experiments.

First of all, the Boussinesq approximation and a slab geometry have been adopted to describe the dynamics of the stratified fluid. Furthermore, to model the oscillating grid used in the experiments, we introduce an external force localized in the upper layers. We shall use dimensionless quantities (x, y and z being the horizontal and vertical coordinates, v_x, v_y and v_z the horizontal and vertical velocities, P the pressure and t the time). The units of temperature, velocity space and time are, respectively, $\bar{v}$, a typical velocity, $\bar{L}$ the vertical depth of the layer, $\bar{T}$, a characteristic temperature, and $\bar{L}/\bar{v}$, the characteristic time. We have used an aspect ratio of 2π. Then, the governing equations read:

$$\frac{\partial \mathbf{v}}{\partial t} = -\mathbf{v}\cdot\nabla\mathbf{v} - \nabla p + R_i\theta\mathbf{e_z} + \frac{1}{Re}\nabla^2\mathbf{v} + \mathbf{F} \tag{1}$$

$$\frac{\partial T}{\partial t} = -\mathbf{v}\cdot\nabla T + \frac{1}{RePr}\nabla^2 T, \tag{2}$$

$$\nabla\cdot\mathbf{v} = 0, \tag{3}$$

where

$$\theta = T - < T >,$$

is the temperature fluctuation with respect to the horizontally averaged temperature $< T >$. The external force we have used has components

$$\begin{aligned} F_x &= (\frac{2}{\sigma}(1-z)^2 - 1)e^{-(1-z)^2/\sigma} \\ &\quad \sum_{k=1}^{N_x} \frac{a_k}{k} sin[kx + \phi_k(\Delta t, \Delta y)], \\ F_y &= 0, \\ F_z &= (z-1)e^{-(1-z)^2/\sigma} \\ &\quad \sum_{k=1}^{N_x} a_k cos[kx + \phi_k(\Delta t, \Delta y)]. \end{aligned} \tag{4}$$

The ϕ_k are random phases distributed uniformly in the interval $[0, 2\pi]$. These phases are taken to be constant on domains $[t_n, t_{n+1}] \times [y_l, y_{l+1}]$ in the (y,t) plane, the times t_n and the points y_l being distributed with a Poisson statistics with mean values Δt and Δy.

Run		α	R_i	N^2	Δt	Δy	u_e^{max}
I	2D	4.0	1.0	4.0	∞		0.040
II	2D	2.0	1.0	2.0	∞		0.060
III	2D	1.0	1.0	1.0	∞		0.075
IV	2D	0.5	1.0	0.5	∞		0.095
V	2D	2.0	0.1	0.2	∞		0.114
VI	2D	1.0	0.1	0.1	∞		0.115
VII	2D	10	0.01	0.1	∞		0.115
VIII	2D	0.5	1.0	0.5	1.2		0.1
IX	2D	0.5	1.0	0.5	0.2		0
X	3D	0.5	1.0	0.5	∞	∞	0.038
XI	3D	0.5	1.0	0.5	0.2	∞	0
XII	3D	0.5	1.0	0.5	1.2	∞	0.041
XIII	3D	0.5	1.0	0.5	1.2	1.5	0.035
XIV	3D	0.5	1.0	0.5	1.2	0.2	0.033

Table 1

In the above equations, $\sigma^{1/2}$ is the vertical extent over which the external force is active, and R_i, R_e and P_r are respectively the normalized Richardson, Reynolds and Prandtl numbers,

$$R_i = N^2\left(\frac{\partial v}{\partial z}\right)^{-2}, \quad R_e = \bar{v}\bar{L}/\nu, \quad P_r = \nu/\kappa,$$

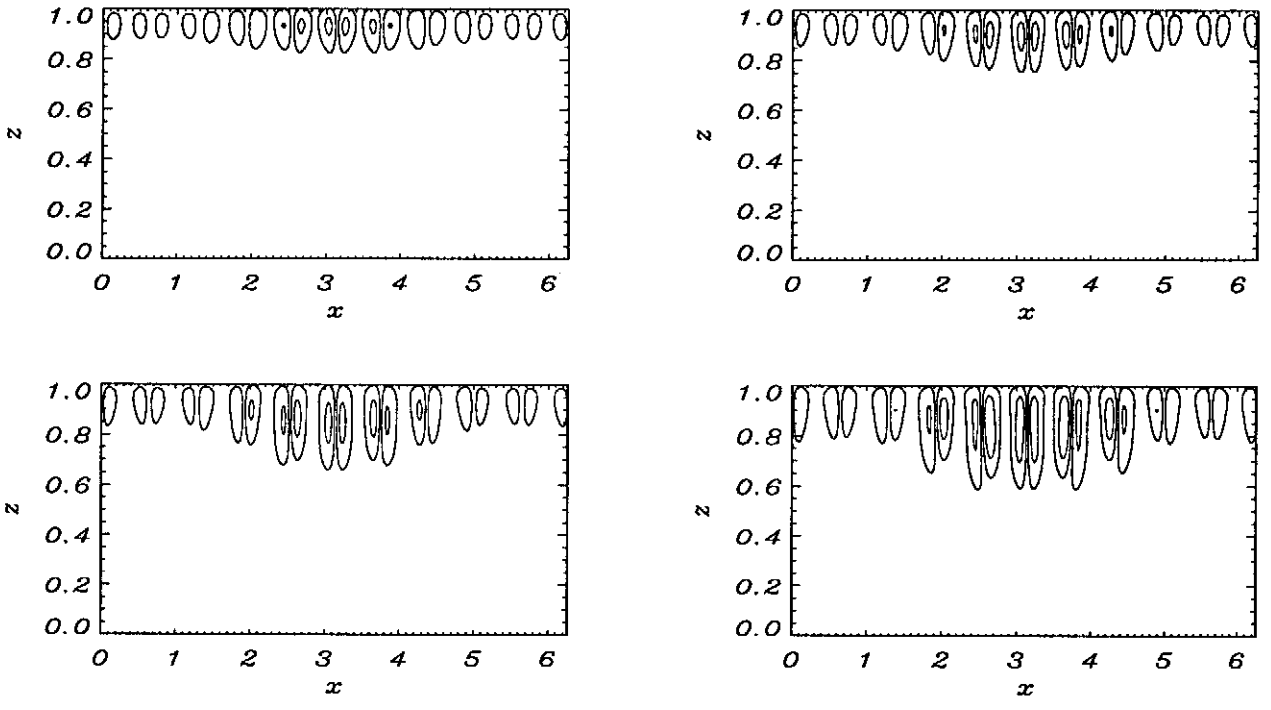

Fig. 1. Contour plot of the stream lines at t=1,2,3,5 (*Run III*).

where N is the Brunt-Vaisala frequency, ν the kinematic viscosity and κ the thermal diffusion.

The layer is bounded by two undeformable plates along which the fluid is allowed to flow freely and through which flows a fixed heat flux. The corresponding boundary conditions are:

$$\frac{\partial v_x}{\partial z}(x,y,0,t)=0, \quad \frac{\partial v_x}{\partial z}(x,y,1,t)=0,$$

$$\frac{\partial v_y}{\partial z}(x,y,0,t)=0, \quad \frac{\partial v_y}{\partial z}(x,y,1,t)=0,$$

$$v_z(x,y,0,t)=0, \quad v_z(x,y,1,t)=0,$$

$$\frac{\partial T}{\partial z}(x,y,0,t)=\alpha, \quad \frac{\partial T}{\partial z}(x,y,1,t)=\alpha.$$

Finally, periodic boundary conditions are imposed in the horizontal directions.

The initial conditions represent a stratified quiescent fluid filling the simulation box,

$$T(t=0)=1+\alpha z, \quad \mathbf{v}(t=0)=0.$$

Note that in the model described above, no mean velocity shear is present at the initial time. This choice is due to the fact that we want to isolate, if possible, the mechanism of conversion of mechanical energy into potential energy when only the external upper energy source is present. In fact, the mean shear, being another possible source, can in principle alter substantially the physics at the interface boundary.

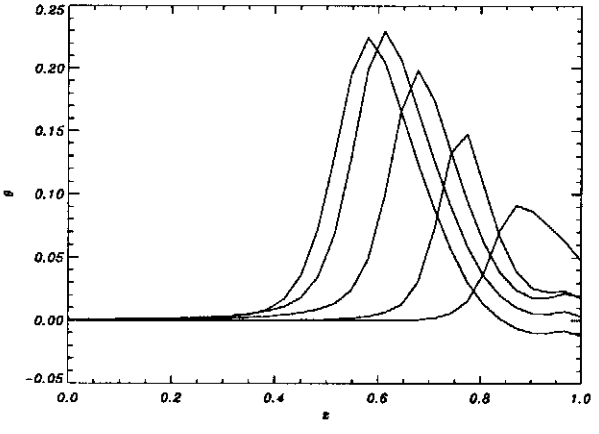

Fig. 2. Vertical profile of temperature fluctuation inside a jet (*Run III*), at $x = 0$.

Finally, in all the runs described here, we have fixed the nominal Reynolds and Prandtl numbers,

$$R_e = 1000\ (2D\ runs), \quad R_e = 500\ (3D\ runs), \quad P_r = 0.5$$

and for the forcing terms, we have always taken the same value of $\sigma = 0.01$, and only three horizontal harmonics,

$$a_{10}=4, \quad a_{11}=2, \quad a_{12}=1,$$

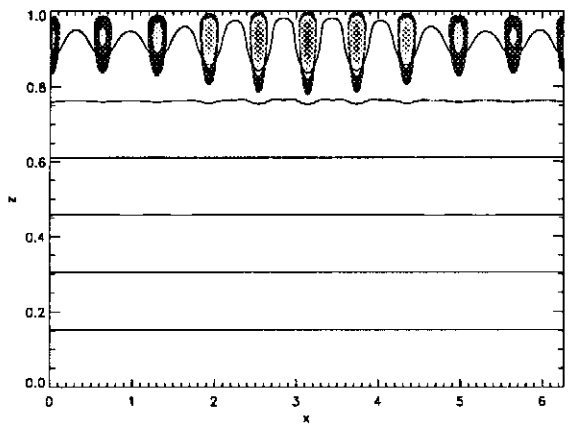

Fig. 3. The solid lines are the isotherms $T = 1.15, 1.3, 1.45, 1.6, 1.75, 1.9$ at t=1; The shaded areas represent levels of downwards vertical velocitiey; there are four levels of gray, the smallest velocities designed by black and the highest, found in the jet centers, by the dark gray (*Run III*).

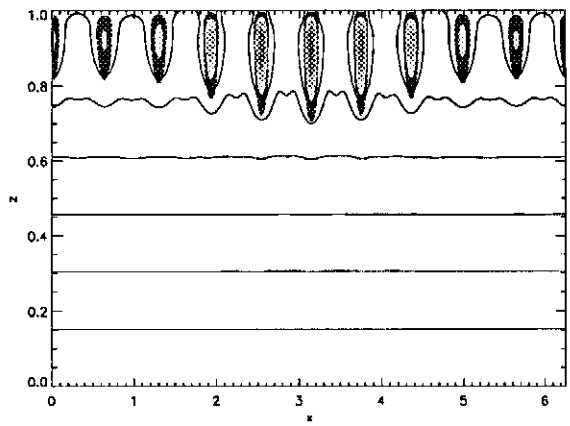

Fig. 4. Same as Fig. 3 at t=2; isotherms are: $T = 1.125, 1.25, 1.375, 1.5, 1.625, 1.75, 1.875$

so that there is one leading amplitude characterizing the force. The typical horizontal scale of the force is $k_x = 10$, while for the vertical one we assume $k_z \simeq (\sigma)^{-1/2} = 10$.

In table 1 we show the values of the other parameters in the various runs described in this paper. In particular, runs $I - IX$ are restricted to the two dimensional case (x, z), while runs $X - XIV$ are three dimensional.

Details about the numerical methods employed are described in the appendix.

3 Results

In the case of a weak external forcing ($a_k \ll 1$), the observed motion is the superposition of *i*) the field of internal waves which are generated by the impulsive start of the force at $t = 0$ and *ii*) the stationary solution $\mathbf{v}_\infty$, T_∞, resulting from the balance between the external forcing and viscous forces. Note that the internal waves propagate in the vertical direction with a vertical group velocity and damping time

$$v_g \simeq 0.035(\alpha R_i)^{1/2}, \quad t_{damp} \sim 5,$$

and that the asymptotic solution which is reached for $t > 5$, is localized in the upper layers, where the force is active.

3.1 Coherent forcing

We shall say that the forcing is coherent when the external force does depend neither on time nor on the transversal coordinate y, i.e. $\phi_k = const$ (see equations 4). When a strong coherent forcing ($a_k \sim O(1)$) is applied to the fluid, one observe the penetration of the motions into the quiescent fluid. These vertical motions, develop far away of the forcing region after a characteristic time $t_c \sim 1$ which is short compared with the characteristic time of propagation of internal waves.

In figure 1 the evolution of the stream lines at four different time instants ($t = 1, 2, 3, 5$), are plotted in the (x, z) plane in the case of Run *III*. In this figure it can be noticed that the vertical motions are organized in very thin jets of horizontal dimension $l_{jet} \sim 0.6$. Inside these structures, but far from the downwards end of the jets, the buoyancy term is negligible due to the fact that the initial vertical temperature gradient has considerably decreased. From a detailed numerical estimate of the various terms in the equation of motion (1), it can be shown that the term which largely dominates in the expression of the vertical acceleration inside these structures is the inertial one,

$$\frac{\partial v_z}{\partial t} \simeq -v_z \frac{\partial v_z}{\partial z}.$$

At the end of the jets, i.e. near the interface, the downward motions are braked by the buoyancy force. The vertical profile (see figure 2) of the buoyancy takes the form of a gaussian profile, localized at the end of the jet, which travels at a more or less constant speed towards the bottom of the box, as can be appreciated in figure 2.

The development of these vertical motions directly produces the distortion of the isotherms. In fact, inside the jets, the equation for the temperature field (2) is largely dominated by the advection term,

$$\frac{\partial T}{\partial t} \simeq -v_z \frac{\partial T}{\partial z}.$$

In figure 3,4,5,7 the evolution of the isotherms is plotted for the same time instants of figure 1; in this figure the shaded plots represent the regions of downwards v_z in order to outline the correlation between the vertical velocity field and the distortion of the isotherms.

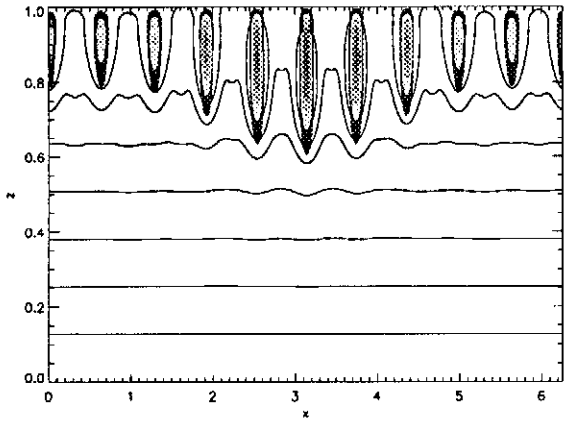

Fig. 5. Same as Fig. 3 at t=3.

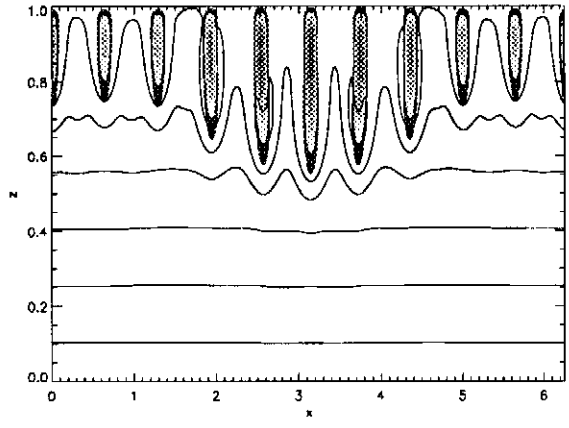

Fig. 7. Same as Fig. 3 at t=5; isotherms are: T= 1.1, 1.25, 1.4, 1.55, 1.7, 1.85.

At this stage, it is worthwhile to notice that the boundary of a jet structure is characterized by very fine scales in the horizontal direction, much smaller than the initial one, $\lambda = k^{-1} = 0.1$, induced by the forcing term. In these region, the diffusive term,

$$\frac{1}{RePr}\frac{\partial^2 T}{\partial z^2},$$

becomes very large.

In figure 6 the temperature is displayed as a function of x, z at $t = 5$; this figure illustrates the reduction in the vertical gradients inside the jets, and the horizontal smoothing of the temperature in the region upwards of the interface.

In figure 8, the horizontally averaged profiles of T, E_{kin} and θ are plotted versus z every $\Delta t = 0.5$. It can be noticed that (a) the initial linear stratification have been completely flattened in a few normalized time in a region much deeper than that where the external forcing is active. The kinetic energy (b) penetrates at an almost constant rate together with the temperature fluctuations until $t \sim 5$. After this time, the penetration is decelerated due to the fact that almost all the injected energy is now dissipated before reaching the interface, so that there is not enough energy to continue the process discussed above.

The results discussed above are restricted to a 2D geometry (the plane (x, z)). To study the influence of 3D motions on the mixing process, in run X (see Table 1) we maintain the same type of energy injection, while three dimensional motions are allowed. In this case, the main result is that the characteristic jet structures observed in the 2D investigations persists. The characteristic formation time of the jet is still $t_c \sim 1$, and the horizontal small scale structure are also present at the boundary of the jets like in 2D geomctry. In figure $9a$, $9b$ the mean temperature field is plotted every $\delta t = 1$ respectively in the case of run IV and run X. Notice that the quantitative difference between these two figure is due to the different values of the Reynolds numbers in the

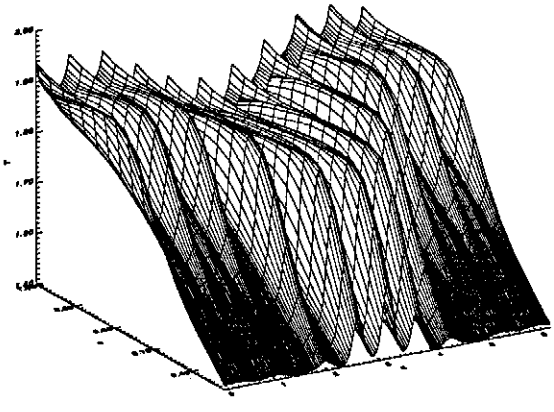

Fig. 6. Temperature field at t=5 (*Run III*).

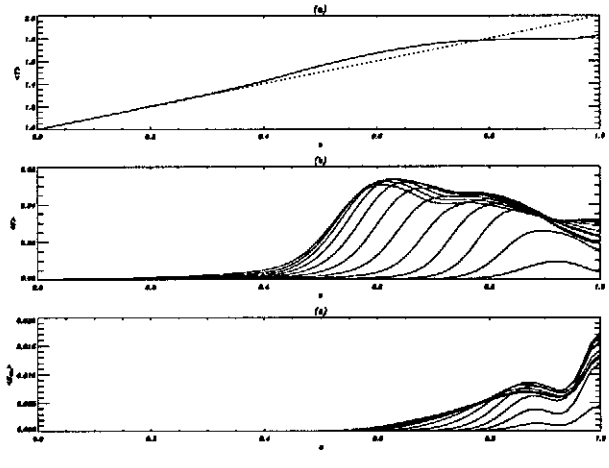

Fig. 8. Horizontally averaged temperature (a), temperature fluctuation (b) and kinetic energy (c) (*Run III*).

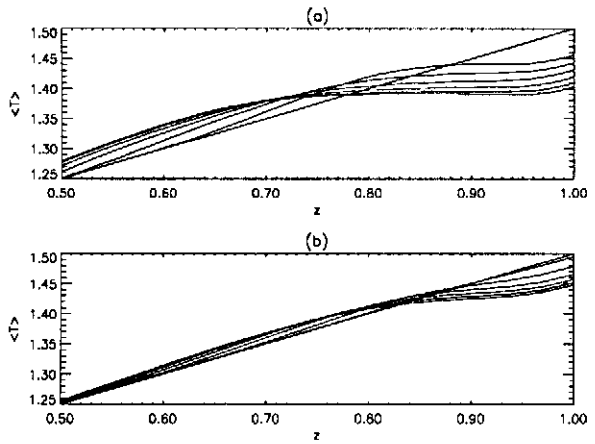

Fig. 9. Horizontally averaged temperature for Run IV (a) and Run X (b).

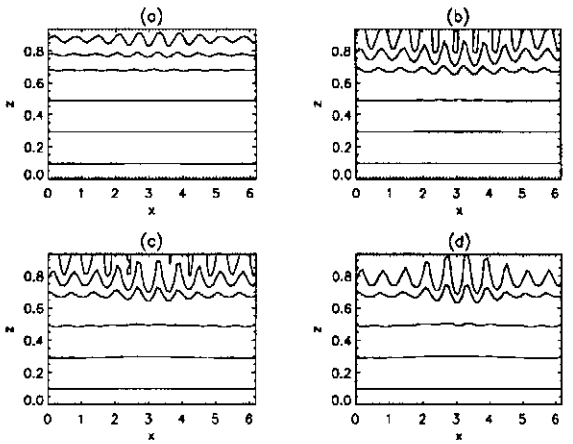

Fig. 11. The isotherms at $y = \pi$, $T = 1.05, 1.15, 1.25, 1.35, 1.4, 1.45$ at times t=1 (a), t=2 (b), t=3 (c), t=4 (d) for Run XII.

two runs.

3.2 Non-coherent forcing

Consider now the case when the external forcing is truly three dimensional, i.e. when Δt becomes comparable with t_c and Δy with the width of a plume (see equations 4).

When the mean time of coherence $\Delta t \sim 0.2 << t_c$ (run XI), no mixing occurs at all whatever is the value of Δy. In particular, motions are confined to the region of forcing, jet structures are not created and the initial temperature gradient remains practically unchanged after a time $t \sim 10$.

When the mean time of coherence (run XII) is of the order of the characteristic time of the dynamics observed in the case of a coherent forcing ($t_c \sim 1$), the numerical results indicate that all the major features observed in the coherent case (runs IV and X) are not changed. In figure 10a and 10b, the mean temperature profile is plotted every $\delta t = 1$ in the case of, respectively, run X and run XII. In figure 11, the isotherms (run XII) are plotted at times $t = 1, 2, 3, 4$ at a fixed y to show the vertical distortion of the temperature field due to the formation of the plumes which, as discussed before, advect the temperature.

In runs $XIII$ and XIV we investigate the case when the coherence length Δy is smaller than the box length, and $\Delta t \sim t_c$. In particular, we investigate the case where the mean value of space uncoherence is of the order (run $XIII$) of the typical dimension of a jet ($\Delta y \sim l_{jet} = 0.6$) or much less (run XIV) than the width of a jet ($\Delta y \sim 0.2$). Both runs show that this spatial uncoherence does not affects the formation and evolution of the plumes, the consequent temperature advection and small scale horizontal structures, and finally the penetration of motions and mixing of the upper fluid.

In figure 12a and 12b, the mean temperature is plotted every $\delta t = 1$ for run IV and XIV. This figure

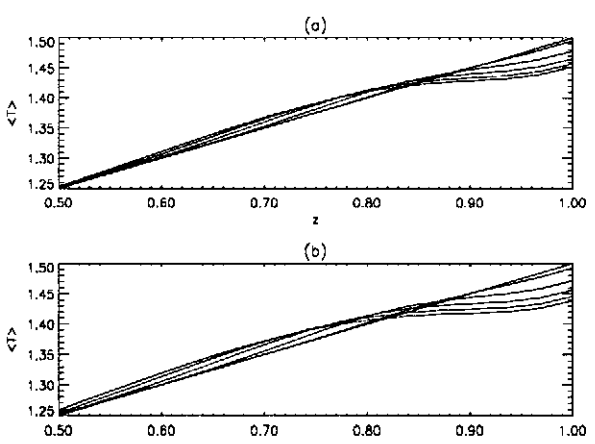

Fig. 10. Horizontally averaged temperature for Run X (a) and Run XII (b).

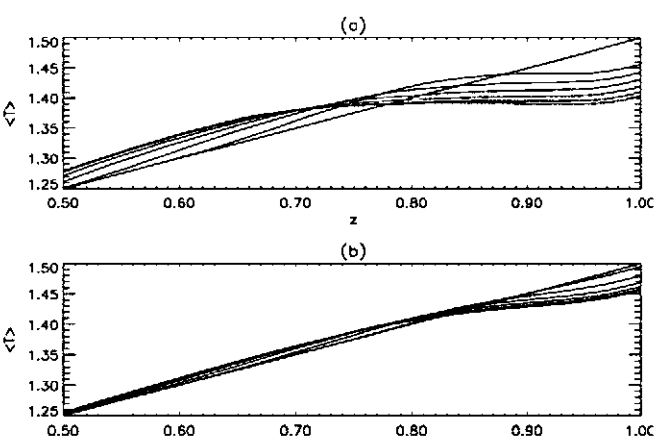

Fig. 12. Horizontally averaged temperature for Run IV (a) and Run XIV (b).

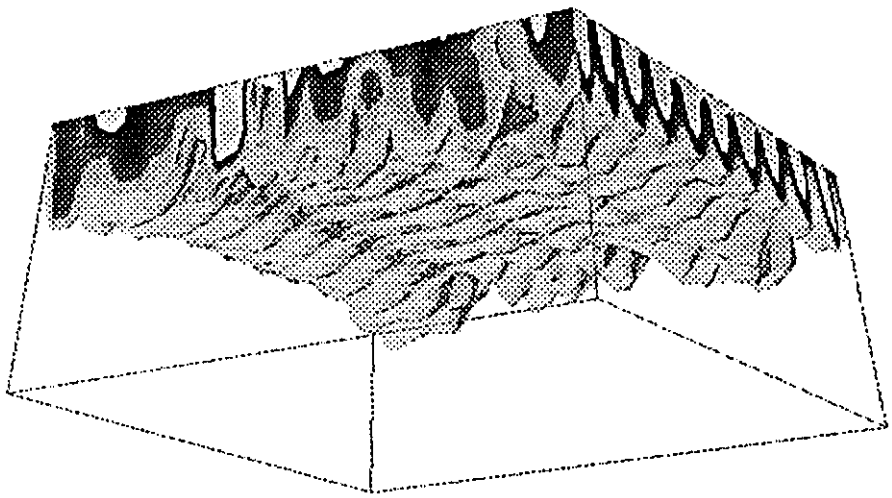

Fig. 13. This figure represents the three dimensional temperature field by showing the volume where the temperature lies in the range $1.35 < T < 1.45$; the level of grey indicates the temperature with black corresponding to the highest temperatures ($T \sim 1.45$).

shows that the results obtained in $2D$ are not changed substantially when a non-coherent forcing with $\Delta t \sim t_c$ and $\Delta y << l_{jet}$ is applied, the only difference being in the entrainment velocity. Nevertheless, the variation of the entrainment velocity is a direct consequence of the smaller Reynolds number used in the 3D run, and not the signature of a different physical process.

In figure 13, we show the isotherms at $t = 6$ in the case of run XIV; we notice, at the edge of the simulating box, that the elongated jet structure are of almost constant temperature; the phase variation in the y directions is on a scale much smaller than the typical width of a jet (l_{jet}). In figure 14 (run XIV) the vertical downwelling velocity also traces the jet like structures which characterize the flow observed in the numerical simulations.

Finally, in all the runs performed, we did found no trace of internal waves involved in the process of mixing, neither at the interfacial level where these waves could, in principle, radiate away a fraction of the kinetic energy to be converted in potential energy.

4 Discussion

The qualitative interpretation of the numerical results discussed in the precedent Section, can be summarized as follows.

First of all, due to the horizontal inhomogeneous character of the forcing term, a local irreversible process of flattening of the vertical gradient of the temperature takes place in the regions where, initially, the vertical velocity field dominates. This advection process, driven by the term,

$$v_z \frac{\partial T}{\partial z},$$

is strongly non-linear, but coherent.

There are two basic effects produced by this mechanism. The first one, is that the buoyancy term, which in generally prevents the system from vertical motions, is locally inhibited; vertical motions pushed by the inertial term

$$v_z \frac{\partial v_z}{\partial z},$$

penetrate into the quiescent fluid down to continue the advection process in the deeper layers where buoyancy is still active. The second effect, which is also strongly non-linear, is the generation of very high gradients in the horizontal direction, so that diffusion becomes very efficient. In this way, the horizontal diffusion produces the final (real) mixing of the fluid on time scales much shorter than the dissipative time scale of the wavelength of the force.

It is worth to notice that the physical mechanism discussed above, which is characteristic of a 2D geometry, remains practically unchanged when three dimensional motions are allowed; in other words, the possibility of

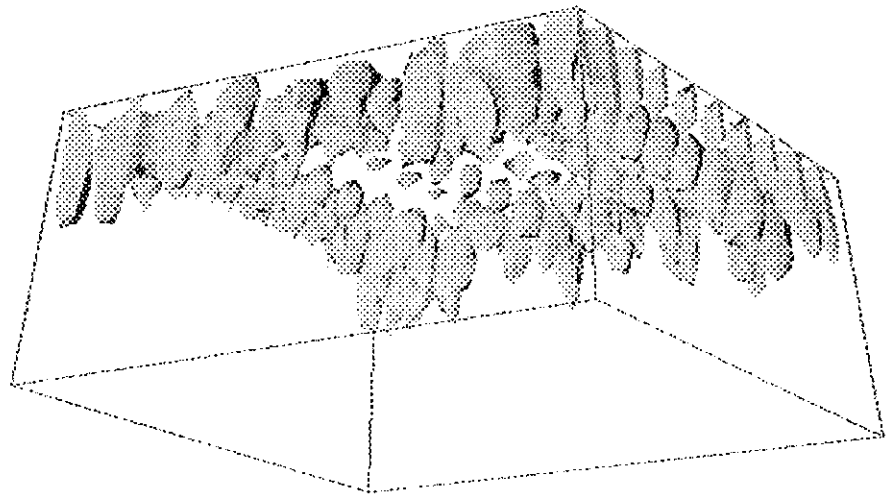

Fig. 14. Same as figure 10 for the vertical downwelling velocity field ($-0.5 < w \sim -0.1$); the level of grey indicates the downwelling velocity with black corresponding to the highest velocity (w$\sim$ -0.5).

developing motions in the direction perpendicular to the plane (x, z) does not destroy the plumes and does not inhibit the formations of very small horizontal scales which are responsible of the horizontal mixing.

One point of particular relevance in the discussion above, is the fact that the process of mixing outlined with the help of the numerical results, being of non-linear nature, is a completely coherent mechanism.

To investigate the effects related to the coherence of the external forcing, we have introduced, first, a time dependent phase showing that, if the typical time of coherence (i.e. the time during which the phase remain unchanged) is greater or of the order of the characteristic time t_c of the dynamics of the plumes, the main qualitative and quantitative features of the coherent case persist. On the other hand, if the time of coherence is shorter than t_c, the results are completely changed and, in particular, plumes are not formed and no mixing is observed. For this reasons we argue that, in the space of parameters of our investigation, the plume structure is a feature essential to produce the mixing of the fluid and the penetration of the kinetic energy in the underlying quiet fluid.

As a second step, we investigated the case in which the coherence of the forcing is destroyed in the direction perpendicular to the plane where plumes are formed. In particular, we introduced a phase with a typical length of coherence along y of the order, or much less, than the typical width of the plumes. In both case we observe that this spatial coherence does not affects substantially the formation of the plumes and the related mixing.

Finally, to reach a more turbulent regime one should increases considerably the Reynolds number, which could in principle change the physics of the mixing of the fluid. Nevertheless, one may hope that in the presence of more turbulent motions, the main result of local advection of temperature and of formation of plumes, should remains.

5 Conclusions

We have presented the first results of a numerical study of the problem of the generation and evolution of a mixed layer in a stably stratified fluid. One of the main outcome of the experiments (Breidenthal 1992) is the scaling of the entrainment rate U with the Richardson number (it should be noted that there is some ambiguity in the definition of R_i in the literature). In the numerical experiments, the definition of the interface is rather loose and so is the definition of its downwards velocity. The comparison with laboratory experiments is therefore very difficult. However, to study the scaling of the entrainment velocity u_e with the strength of the stratification, we have chosen to use as entrainment velocity the velocity with which the maximum of the vertical gradient of the mean temperature propagates downwards.

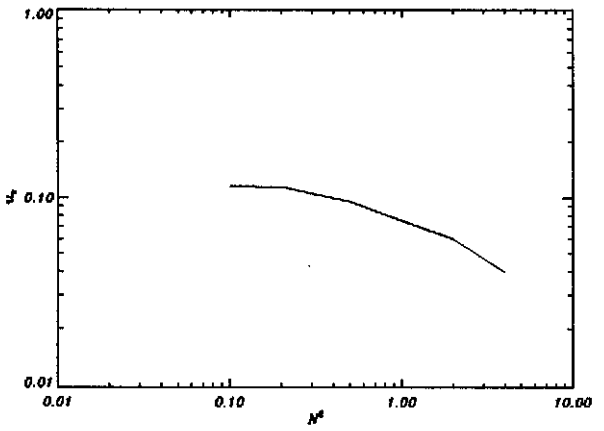

Fig. 15. Entrainment velocity versus Brunt-Vaiasala frequency.

This velocity is not really constant (within a factor of two), and in figure 15 its maximum value is plotted against N^2 for the runs $I - VIII$ of Table 1 which have the same nominal Reynolds number, $R_e = 1000$. For "small" values of N^2, the entrainment velocity does not change significantly, while at larger values it scales as N^{-1}. This behaviour is qualitatively in agreement with the laboratory experiments, except that the power law is different. This may be a consequence of the fact that the effective Reynolds number reached in our simulations are much less than that of the experiments. As already stated above, one may hope that this difference in the Reynolds number should not change qualitatively the physical mechanism discussed in the paper, while the results should change quantitatively for a Reynolds numbers smaller than a critical one. A quantitative variation of the entrainment velocity can be noticed in Table 1 going from 2D to 3D runs. This is due to the fact that, for numerical resolution problems, we have reduced by a factor of two the nominal Reynolds number in 3D runs what, as a consequence, reduces the downwelling velocity inside the plumes and so the advection mechanism. It is possible to think that, when increasing the Reynolds number, there is a maximum value of the velocity corresponding to $R_e = R_e^{crit}$ after which the characteristic velocity inside the jets does not vary significantly for greater values of R_e, so does u_e.

In these simulations, the physical mechanism which is responsible of the mixing of the fluid appears now sufficiently clearly. This mechanism, which could be summarized as a "non-linear advection" and which is discussed in Sections 3 and 4, is, as far as we know, original in this context.

In the discussion of the numerical results, Section 3, and of their interpretation, Section 4, it has been pointed out that no signature of internal waves in the mixing process or in removing kinetic energy from the interface, were found.

Finally, we may speculate about the fact which can be expected if the fluid is no longer incompressible. Numerical simulations of compressible convection have shown a strong asymmetry between small scales downwelling velocities and large scale slow upwelling velocities, similiar to what is observed in the simulations described here. Thus, it is natural to expect that compressibility will amplify this asymmetry.

6 Appendix: Numerics

The choice of the numerical algorithm is mainly based on the need to solve the propagation of very strong gradient at the interface boundary and the nonlinear interactions present in the mixed region. Nevertheless, the peculiarities of the super computer to be used to run the code must also be taken in consideration. The code runs on a Connection Machine, a massively parallel computer with at least 8192 processors (see Califano & Mangeney, 1994, Califano 1994) for a more detailed discussion about the numerical algorithm).

To advance in time the fields $\mathbf{u}$ and T we use the explicit algorithm *Adams Bashford III* with an accuracy $O(\delta t^3)$.

Let assume that we know the temperature and velocity field at the instant n, and let define $\mathbf{H}^m$ and $\mathbf{Q}^m$ the right hand sides of equation (1) and (2),

$$\mathbf{H}^m = \left\{ -\mathbf{u}\cdot\nabla\mathbf{u} + R_i\theta\,\mathbf{e}_z + \mathbf{F} + \frac{1}{Re}\nabla^2\mathbf{u} \right\}^m,$$

$$Q^m = \left\{ -\mathbf{u}\cdot\nabla T + \frac{1}{R_e P_r}\nabla^2 T \right\}^m,$$

which are known at the instant $n-2$, $n-1$, and n. The new temperature field is calculated as:

$$T^{n+1} = T^n + \delta t \left[\frac{23}{12}Q^n - \frac{4}{3}Q^{n-1} + \frac{5}{12}Q^{n-2} \right], \qquad (5)$$

To calculate the velocity field at the time step $n+1$, we introduce an intermediate step, $\mathbf{u}^*$,

$$\mathbf{u}^* = \mathbf{u}^n + \frac{23}{12}\delta t\mathbf{H}^n + \delta t\left[-\frac{4}{3}\left(\mathbf{H}^{n-1} - \nabla P^{n-1}\right) + \frac{5}{12}\left(\mathbf{H}^{n-2} - \nabla P^{n-2}\right) \right]. \qquad (6)$$

The actual velocity field at the instant $n+1$, is calculated as

$$\mathbf{u}^{n+1} = \mathbf{u}^* - \frac{23}{12}\delta t\,\nabla P^n, \qquad (7)$$

where the pressure P^n is obtained by solving the Poisson equation

$$\nabla^2 P^n = \frac{12}{23\delta t}\nabla\cdot\mathbf{u}^*, \qquad (8)$$

which is obtained by imposing $\nabla \cdot \mathbf{u}^{n+1} = 0$ on equation (7).

In the equations (5)-(8) the presence of the intermediate step to calculate $\mathbf{u}^*$, allows to eliminate the accumulation of the "compressible" numerical error, i.e. the numerical error which leads to a non vanishing velocity divergence.

To calculate the spatial derivatives necessary to compute $\mathbf{H}^m$ and Q^m, we use spectral methods (FFT) in the (x, y) plane, while non-linear terms are calculated in the physical space.

On the vertical inhomogeneous direction we use a method, known as compact finite differences (CFD) (Lele, 1992), which allows us to provide an accurate description of a wide range of spatial scales (not far from spectral methods), while keeping the flexibility of all finite difference methods for non periodic situations. In particular, in our code, we use a CFD scheme of eight order for which the truncation error when calculating the first derivative of a generic function f is

$$\Delta\epsilon_1 = \frac{16}{9!} dz^8 \frac{d^9 f}{dz^9},$$

while for the second derivative

$$\Delta\epsilon_2 = 3 \cdot 10^{-5} dz^8 \frac{d^{10} f}{dz^{10}}.$$

The Poisson equation is solved by first making a Fourier Transform along the horizontal (periodic) axis x and y, using CFD methods to solve the resulting ordinary differential equations for $P_{l,j}(z)$ in the inhomogeneous direction, and finally back in the physical space with inverse Fourier Transform along axis x and y.

Finally, the boundary conditions on the vertical velocity ($v_z(0,1) = 0$), are introduced via the pressure field. In fact, when solving the Poisson equation (8), the boundary conditions are

$$\frac{\partial P^n}{\partial z} = \frac{12}{23\delta t} v_z^*,$$

which automatically implies, equation (7), that v_z^{n+1} should vanish in $z = 0, 1$.

Acknowledgements. We are pleased to acknowledge Thinking Machine Corporation and Scuola Normale Superiore of Pisa for providing us the facilities of their computing centers (CMNS, CM-SNS).

One of us (F.C.) acknowledge with pleasure the help of Dr. P.Rossi (Centro ricerca e studi superiori, CRS4) who introduced him to the use of the *Connection machine* and Dr. Kapil Mathur (Thinking Machine Corporation) for numerical suggestions to improve the performance of the numerical code.

We thank the referee for very useful comments which helped to improve the contents of the paper.

Reference

Breidenthal, R.E.: 1992, *Phys. Fluids,***10**, *2141*
Califano, F. *to be submitted to J. Comput. Phys.*
Califano, F., Mangeney, A.: 1994 *to be published by World Scientific*
Dahm, W.J., Scheil, C.M., Tryggvason, G.: 1989, *J. Fluid Mech.,***205**, *1*
Fernando, H.J.S., Long, R.R.: 1985a, *Phys. Fluids,***28**, *2999*
Fernando, H.J.S., Long, R.R.: 1985b, *J. Fluid Mech.,***151**, *21*
Fernando, H.J.S.: 1991, *Annu. Rew. Fluid Mech.,***23**, *455*
Hopfinger E.J., Toly, J.A..: 1975, *J. Fluid Mech.,***78**, *155*
Lele S. K.: 1992, *J. Comput. Phys.,***103**, *16*
Linden, P.F.: 1973, *J. Fluid Mech.,***60**, *467*
Linden, P.F.: 1975, *J. Fluid Mech.,***71**, *385*
Meng J.C.S., Rottman J.W.: 1988, *J. Fluid Mech.,***186**, *419*
Mory, M.: 1991, *J. Fluid Mech.,***223**, *193*
Niiler, P.P.: 1975, *J. Mar. Res.,***33**
Thompson, S.M., Turner J.S.: 1975, *J. Fluid Mech.,***67**, *349*
Turner J.S.: 1968, *J. Fluid Mech.,***33**, *639*
Turner J.S.: 1973, *Buoyancy Effects in fluids*, Cambridge University press
Turner J.S.: 1986, *J. Fluid Mech.,***173**, *431*
X. E, Hopfinger E.J.: 1986, *J. Fluid Mech.,***166**, *227*